Biocompatible Iron Sulphide Nanoparticles Against Neuroinflammation for Intracerebral Haemorrhage and Long-term Neurological Functional Recovery

Song Zhang
Yangzhou University https://orcid.org/0000-0001-9583-3926
Tianqing Xiong
Yangzhou University
Yuan Yuan
Yangzhou University
Wenwen Zhuang
Yangzhou University
Yijun Xu
Yangzhou University
Jingwen Zhang
Yangzhou University
Chunhua Tao
Yangzhou University
Jingyan Liang
Yangzhou University
Zhuobin Xu (xuzb@yzu.edu.cn)
Yangzhou University

Research

Keywords: Intra cerebral haemorrhage, Nanosized iron sulphide, Neuroinflammation, Oxidative stress, Apoptosis

Posted Date: October 11th, 2021

DOI: https://doi.org/10.21203/rs.3.rs-927257/v1

Biocompatible iron sulphide nanoparticles against neuroinflammation for intracerebral haemorrhage and long-term neurological functional recovery

Song Zhang[1#], Tianqing Xiong[2,3,4#], Yuan Yuan[1], Wenwen Zhuang[2], Yijun Xu[2], Jingwen Zhang[1], Chunhua Tao[1], Jingyan Liang[2,3,4*], Zhuobin Xu[2,3*]

[1]School of Nursing, Yangzhou University, Yangzhou, 225001, China

[2]School of Medicine, Yangzhou University, Yangzhou, 225001, China

[3]Institute of Translational Medicine, Medical College, Yangzhou University, Yangzhou, 225001, China

[4]Jiangsu Key Laboratory of Integrated Traditional Chinese and Western Medicine for Prevention and Treatment of Senile Diseases, Yangzhou University, Yangzhou, 225001, China

*Correspondence to：

Zhuobin Xu, Jingyan Liang

Institute of Translational Medicine, Medical College, Yangzhou University, Yangzhou, 225001, China

E-mail: xuzb@yzu.edu.cn, jyliang@yzu.edu.cn

[#]Song Zhang and Tianqing Xiong contributed equally to this work.

Abstract

Background: Mass effects of haematoma, neuroinflammation, oxidative stress, and neuronal apoptosis are the major causes of poor prognosis of intracerebral haemorrhage (ICH). Our previous study suggests that biocompatible iron sulphide nanoparticles possess peroxidase-like activity and can release hydrogen polysulfanes，which may inhibit brain injury. The purpose of this study was to investigate the neuroprotective efficacy of diallyl disulfide (DADS) nFeS in mice after ICH and preliminarily illustrate the potential mechanism.

Methods: Adult male C57BL/6 mice (n = 176) were injected with bacterial collagenase in the striatum. In the first part, DADS-nFeS at different doses (25, 50, or 100 mg/kg) was intragastrically administered 2 h, 26 h, and 50 h before ICH. In the second and third parts, DADS-nFeS (50 mg/kg) was administered 2 h, 26 h, and 50 h before and after the induction of ICH in the pre-treatment group and post-treatment group, respectively. H&E staining was performed to detect drug toxicity. Haematoma volume measurement, Fluoro-Jade C (F-JC) staining, Nissl staining, immunofluorescence staining, western blotting, terminal deoxynucleotidyl transferase dUTP nick end labelling (TUNEL) staining, malondialdehyde (MDA) and superoxide dismutase (SOD) assays, and neurobehavioural tests were performed.

Results: All three doses of DADS-nFeS had neuroprotective effects, and 50 mg/kg resulted in the best outcome. DADS-nFeS reduced the haematoma volume and MDA content, inhibited the activation of microglia and astrocytes, progressive neuronal degeneration, and apoptosis, increased SOD activity and neuronal survival, and improved both short-term and long-term neurological functions in perihaematomal areas after ICH. Moreover, DADS-nFeS was associated with the downregulation of Iba-1, GFAP, TNF-α, IL-1β, 4-hydroxynonenal (4-HNE), and Bax/Bcl-2 levels in perihaematomal areas after ICH. Finally, post-treatment with DADS-nFeS had a better effect than pre-treatment with DADS-nFeS.

Conclusions: Our study indicated that gavage administration of DADS-nFeS decreased the haematoma volume, suppressed neuroinflammation, oxidative stress, and neuronal apoptosis, and improved short- and long-term neurological functions, which was, at least in part, realized by inhibiting the activation of microglia and astrocytes, enhancing local SOD activity, and decreasing the recruitment of reactive oxygen species. Therefore, DADS-nFeS may serve as a potential therapeutic strategy via the diet against central nervous system diseases.

Keywords: Intracerebral haemorrhage, Nanosized iron sulphide, Neuroinflammation, Oxidative stress, Apoptosis

Background

As a serious cerebrovascular disease, spontaneous intracerebral haemorrhage (ICH) accounts for approximately 10–15% of all strokes and is usually accompanied by a high rate of morbidity and mortality[1, 2]. Brain injury after ICH can be mainly classified as primary brain injury (PBI) and secondary brain injury (SBI). Of these, PBI mainly involves the formation of expanding haematoma compressing surrounding brain tissue and cerebral vascular structure, which in turn results in mechanical injury after intracerebral haemorrhage[3]. SBI is induced by the interplay of complicated pathologic responses involving an inflammatory process initiated by blood components, oxidative stress via induction of erythrocyte lysates, and the progressive degeneration or apoptosis of neurons activated by excitotoxicity[4, 5]. Due to the deep location of the cerebral haematoma in the brain and secondary injury after the operation, increasing evidence from clinical trials has revealed that open surgery to remove haematoma does not effectively improve the prognosis of patients[6, 7]. Therefore, the endogenous mechanisms of haematoma evacuation based on SBI warrant further research.

With the development of nanotechnology, nanomaterials have been commonly utilized in the biomedical field due to their nonintrusive and safe features. Because of

the high iron content in the human body, iron-based nanomaterials are considered to be more biocompatible than other metal elements[8]. At present, most iron-based nanomaterials are iron oxides that possess oxidoreductase-like activity. Iron sulphide nanomaterials have received much less attention in the biomedical domain. In fact, however, the band gap in iron sulphide is smaller than that of iron oxide, and iron-sulphur clusters are crucial cofactors of many enzymes[9]. Thus, iron sulphide may show stronger enzyme-like activity and catalytic activity than iron oxide. In our previous study, we confirmed that diallyl disulfide (DADS) nFeS has peroxidase-like activity and can release hydrogen polysulfanes with anti-inflammatory and antioxidant functions. A study showed that reactive oxygen species (ROS) were closely related to inflammatory development in ICH[10]. Therefore, the use of DADS-nFeS as a free radical scavenger and cooperation with hydrogen polysulfane anti-inflammatory and antioxidant stress may have certain developmental prospects.

In this study, DADS-nFeS was administered intragastrically in an experimental ICH model, and haematoma volume, neuroinflammation, oxidative stress, neuronal apoptosis, and neurological deficits were evaluated. Moreover, we explored the neuroprotective effect of DADS-nFeS and its potential mechanisms. To the best of our knowledge, this is the first study to investigate the therapeutic efficacy of nFeS on ICH, which may provide novel ideas for the treatment of ICH.

Methods

Synthesis and Characterization of DADS-nFeS

As previously described, DADS-nFeS was synthesized with the typical solvothermal method[11]. We determined the morphological and structural characteristics of DADS-nFeS. The products were stored in test tubes and refrigerated at 4 ℃ for further use.

Animals

All experimental procedures were in accordance with the National Institutes of Health

Guidelines for the Care and Use of Laboratory Animals and approved by the Yangzhou University Institutional Animal Care and Use Committee. Adult male C57BL/6 mice (postnatal week 8) were purchased from the Comparative Medicine Center of Yangzhou University, and mice weighing 25–35 g were selected for induction of intracerebral haemorrhage after one week of adaptation. All mice were housed under a 12 h light/dark cycle and had free access to water and food in a controlled environment of temperature (22 ± 3 °C) and humidity (60 ± 5%). All mice were randomly assigned to the experimental and control groups following a random number table.

Experimental design

A total of three separate experiments were performed, and experimental groups were established (Figure 1). Before intragastric treatment, the mice were randomly divided into a control group, cerebral haemorrhage group and different pre-treatment and post-treatment groups. Before and after the induction of intracerebral haemorrhage, mice in the ICH group and the intervention group were given three gavages. Only animals that died before being sacrificed were excluded from the experiment. (A total of 18 animals were excluded from the experiment.) Neurobehavioural functional evaluation was performed and histological images were collected in a blinded manner.

Experiment 1

To evaluate the toxicity and compare the effects of treatment at different dosages on mice, we established DADS-nFeS groups with three different doses. For the effects of the drug 72 h after ICH, 60 mice were assigned to five groups: sham, ICH + vehicle, ICH + DADS-nFeS (25 mg/kg), ICH + DADS-nFeS (50 mg/kg), and ICH + DADS-nFeS (100 mg/kg) (n = 12/group). H&E staining was conducted to detect the perceived pathological change in the major organs. Slices obtained from the brain mould (G1137101-002, RWD, China) were used to measure the changes in haematoma volume. F-JC staining and Nissl staining allowed the identification of

degenerating neurons and neuronal Nissl bodies.

Experiment 2

To assess the effects of DADS-nFeS administration on neuroinflammatory factors, microglial/astrocytic activation, oxidative stress, apoptotic neurons and neurobehavioural function at 72 h after ICH, we randomly divided 72 mice into four groups for immunofluorescence, western blotting analysis, SOD and MDA assays, TUNEL staining, and neurobehavioural tests: sham, ICH + vehicle, ICH + DADS-nFeS (50 mg/kg, pre-treatment), and ICH + DADS-nFeS (50 mg/kg, post-treatment) (n = 18/group).

Experiment 3

To investigate the effects of COG1410 on long-term neurobehavioural functions after ICH, we assigned 24 mice to four groups: sham, ICH + vehicle, ICH + DADS-nFeS (50 mg/kg, pre-treatment), and ICH + DADS-nFeS (50 mg/kg, post-treatment) (n = 8/group). The rotarod test and Y maze were performed on Days 7, 14, and 21 after ICH. The Morris water maze was conducted on Days 21–25 after ICH.

ICH model

As previously described[12], cerebral haemorrhage was induced by stereotactic collagenase injection into the right basal ganglia in the experimental mice. First, we anaesthetized the mice via 1–3% isoflurane inhalation and immobilized them on a brain stereotaxic apparatus in the prone position. The scalps were expanded to expose the skull, and we took the bregma position as the coordinate origin. A hole 1 mm in diameter was drilled that was 0.5 mm forward and 2.5 mm right lateral to the origin, and bacterial collagenase (Type IV, Sigma-Aldrich, USA) was injected at a depth of 3.8 mm at a rate of 0.04 μL/min for 5 min. After the injection, the needle was kept at the injection point for 10 min to prevent liquid backflow and then removed slowly. Finally, bone wax was used to close the cranial pinhole, and the incisions in the skin

were sutured. Each mouse was intraperitoneally injected with 0.4 mL of normal saline to avoid postoperative dehydration. The mice in the sham group only received needle insertion.

Gavage administration

For the pre-treatment and post-treatment groups, gavage administration was performed 2 h, 26 h, and 50 h before and after ICH, respectively. PBS or DADS-nFeS at three different dosages (25 mg/kg, 50 mg/kg, and 100 mg/kg) dissolved in PBS was administered via gavage. Briefly, each mouse was gavage-fed with approximately 0.32 mL of solution.

H&E staining

For H&E staining, samples of the heart, liver, spleen, lung, and kidney were collected and then fixed in 4% paraformaldehyde (PFA) for 24 h. After the samples were embedded and sliced, they were stained with H&E after dehydration. Finally, morphological changes were observed under a Nikon Eclipse Ni-U upright microscope to evaluate histological damage.

Fluoro-Jade C staining

Fluoro-Jade C staining is usually performed to visualize degenerating neurons and has been identified as a reliable indicator. The brain tissues were sliced into 30-micrometer-thick frozen sections and collected in 0.1M PBS. All tissue slices were dried for at least 1 h at 60 °C before staining. Slices were then immersed in a solution of 1% NaOH and 80% alcohol for 5 min, followed by rinsing in 70% ethanol and double distilled water for 2 min. After transfer to 0.06% potassium permanganate solution for 10 min on a shaker, the sections were incubated in 0.0004% F-JC (AG325, Millipore, USA) solution for 20 min. The slides were then washed in double distilled water and dried at 60 °C for 3 min. Finally, the slides were cleared in xylene for 1 min and affixed to using D.P.X (BCCC7767, Sigma-Aldrich, USA). Sections were

immediately observed, and fluorescence images were captured using Carl Zeiss Microscopy (Axio Scope A1, Germany).

Nissl staining

Viable neurons were observed via Nissl staining for 72 h after ICH. As previously described [13], the slides were pretreated in chloroform for 30 min, hydrated in graded ethanol solutions (100–70%) in distilled water, and stained with cresyl violet acetate (C5042, Sigma-Aldrich, USA) for 90 min at room temperature. Subsequently, the brain slices were washed with double distilled water 3 times and dehydrated through an alcohol series (70–100%). Finally, the sections were cleared in xylene and covered with neutral resin. ImageJ software was used to count the stained neurons.

Immunofluorescence staining

After mice were anaesthetized with 1–3% isoflurane inhalation and intracardially perfused with normal saline and 4% PFA, the brain was removed and fixed in 4% PFA for 24 h at 4 °C and dehydrated in gradient sucrose solutions (5%, 10%, 20%, 30%) for approximately 3 days. The brain tissue was embedded in optimal cutting temperature (OCT) compound, snap-frozen at −80 °C, and sliced into 30-μm-thick coronal sections using a freezing microtome (Leica, Germany). The frozen sections were fixed in acetone for 10 min and incubated with 3% bovine serum albumin (BSA) for 1 h at room temperature. After blocking nonspecific staining, the slices were incubated with primary antibodies, including GFAP (1:100, ab7260, Abcam, USA), Iba-1 (1:100, ab108539, Abcam, USA), and 4-HNE (1:100, MAB3249, R&D Systems, China), overnight at 4 °C. After that, the frozen sections were washed with PBS 3 times and incubated with the corresponding secondary antibodies (Thermo Fisher Scientific, USA) for 2 h at room temperature. Finally, the nuclei were counterstained with DAPI (Beyotime Biotechnology, China), and the slides were affixed to FluorSave Reagent (3429091, Merck KGaA, Germany).

Western blotting

To detect the protein expression levels of different groups, we performed western blotting. The haematoma and its surrounding area were obtained and lysed in 400 μl of lysis buffer containing 4 μl of proteinase inhibitor for 30 min. The extracted sample was centrifuged at 12000 g for 30 min at 4 °C, and the supernatant was collected. After the protein concentration was evaluated by the BCA protein assay kit, an equal amount of protein sample was obtained and then electrophoresed in a 10% SDS-PAGE gel. Then, the protein was transferred to polyvinylidene fluoride (PVDF) membranes (0.22 μm). After being blocked in 5% BSA for 2 h, the PVDF membranes were incubated with primary antibodies, including TNF-α (1:1000, ab6671, Abcam, USA), IL-1β (1:1000, ab9722, Abcam, USA), GFAP (1:1000, ab7260, Abcam, USA), Iba-1 (1:1000, ab108539, Abcam, USA), 4-HNE (1:500, MAB3249, R&D Systems, China), Bcl-2 (1:1000, ab196495, Abcam, USA), Bax (1:1000, ab216494, Abcam, USA), and GAPDH (1:1000, CW0100M, CWBIO, China), overnight at 4 °C. The PVDF membranes were then washed three times with 1×TBST and incubated with secondary antibodies for 1.5 h at room temperature. Protein bands were detected using Tanon 5200 (Tanon, China).

TUNEL staining

TUNEL staining was conducted to quantify apoptosis in intracerebral cells. A TUNEL BrightRed Apoptosis Detection Kit (A113-01, Vazyme, China) was utilized at 72 h after ICH according to the manufacturer's instructions. The data are described as the percentage of TUNEL-positive cells (%).

Measurement of SOD activity and MDA content

According to the manufacturer's certificate, the MDA assay kit (A003-1-2, Jiancheng, China) and SOD assay kit (S0103, Beyotime, China) were used to detect SOD activity and MDA content using supernatants of mouse brains.

Short-term neurobehavioural assessment

As described previously[12, 14, 15], short-term neurological tests were carried out using the corner turn test, forelimb placement test, and rotarod test by two blinded investigators at 24 h and 72 h after ICH. For the forelimb placement test, we recorded the placement of the forelimb contralateral to the haematoma side on the countertop when the vibrissa was stimulated. The percentage of forelimb placement in 10 trials was calculated. For the corner turn test, mice were placed before a 30° angle corner, and the direction the mouse exited was counted. A total of ten trials were performed, and the score was described as the number of right turns/all trials × 100. For the rotarod test, all mice were trained once a day for three days before intracerebral haemorrhage by running on the rotating cylinder at 10 RPM for 30 min. During the test, the rotating speed started at 5 RPM and gradually increased by 2 RPM every 5 s. The selected mice were tested 3 times/day, and the average falling latency was recorded.

Long-term neurobehavioural assessment

As previously reported[16, 17], the rotarod test and Y maze test were utilized to assess sensorimotor coordination and spatial working memory on the 7th day, 14th day and 21st day after ICH, while the Morris water maze was conducted to evaluate the spatial learning ability and reference memory on Days 21 to 25 after ICH. The rotarod test was performed in the same manner as described above. For the Y maze test, a Y-shaped maze with three opaque arms was used, and the mice were allowed to explore freely for 8 min. The total numbers of arm entries were measured by a monitor immediately above the apparatus and analysed by the Supermaze system (XinRuan, China). Alternation percentage (%) was calculated as (successive triplet sets [entries into three arms consecutively]/total number of entries –2] × 100. For the Morris water maze, mice were placed in a metal circular pool that was divided evenly into four quadrants and allowed to find a visible platform above the water level in 60 s. If the mouse did not find the platform within 60 s, it would be guided to stay on the

platform for 10 s to help it remember the location of platform and the swim path, escape latency, and swim distance were recorded individually. Finally, we removed the platform and performed probe trials. The percentage of time that the mouse spent in the target quadrant that previously contained the hidden platform was recorded.

Statistical analysis

All data are presented as the mean and standard deviation (mean ± SD). Statistical analysis was performed using Graphpad prism 8.0 (GraphPad Software, USA). Analysis of variance (ANOVA) was utilized to compare the differences in haematoma volume, immunofluorescence staining, western blotting, assay kit, and neurobehavioural assessment. Differences were considered significant when $p < 0.05$.

Results

Animal exclusion and drug toxicity.

A total of 176 mice were utilized for this experiment. Of these, 138 mice experienced intracerebral haemorrhage, and the mortality of the mice was 6.52% (9/138). In addition, no mice died in the sham group. Three mice were eventually excluded from subsequent experiments and replaced by other animals due to lack of cerebral haematoma. In addition, H&E staining was performed to detect drug toxicity, and no perceived pathological changes were observed in the major organs, which suggested that the three dosages of DADS-nFeS would have no side effects (Figure 2).

DADS-nFeS treatment reduced cerebral haematoma volume and protected viable neurons at 72 h after ICH.

Three different dosages of DADS-nFeS were utilized to select the optimal dose that showed the best effect on intracerebral haemorrhage. First, we quantified the haematoma size in mouse brains at 72 h after ICH via coronal brain mould slices and found that the three groups treated with DADS-nFeS had smaller haematoma volumes than the ICH + vehicle group (Figure 3a, b). Moreover, the best efficacy was observed

in the ICH + DADS-nFeS (50 mg/kg) group versus the other two groups (Figure 3a, b). Distinct degenerated neurons were detected in the ICH + vehicle group at 72 h compared with the sham group, as shown by F-JC staining, while the administration of DADS-nFeS obviously alleviated neuronal degeneration (Figure 3c, d). Similarly, the proportion of degenerated neurons also showed the same trend after treatment with three different dosages. Furthermore, Nissl staining was performed to detect viable neurons at 72 h after ICH. Consistently, ICH + DADS-nFeS (50 mg/kg) significantly reduced the death of neurons and brain injury compared to those of the ICH + vehicle group (Figure 3e, f). Therefore, the middle dosage of DADS-nFeS was chosen for further experiments.

DADS-nFeS treatment inhibited microglial and astrocyte activation and the expression of Iba-1, GFAP, TNF-α, and IL-1β at 72 h after ICH.

To further explore the neuroprotective efficacy of DADS-nFeS after ICH, we detected the distribution of microglia and astrocytes in the perihaematoma area. Immunofluorescence staining was performed to observe the levels of Iba-1 and GFAP at 72 h after ICH. We found that the numbers of Iba-1- and GFAP-positive cells were obviously increased in the ICH + vehicle group versus the sham group, while DADS-nFeS treatment evidently decreased Iba-1 and GFAP clustering in the perihaematomal area compared with that in the ICH + vehicle group (Figure 4a, b, c, d). In addition, western blotting was performed at 72 h after ICH to measure the expression of inflammatory cells and inflammatory factors in the mouse brains. The results showed that the expression of Iba-1 and GFAP in the ipsilateral hemisphere was significantly inhibited by DADS-nFeS in the therapeutic intervention group compared to the ICH + vehicle group (Figure 4e, f, g). The expression of the proinflammatory mediators TNF-α and IL-1β was also reduced in the two ICH + DADS-nFeS groups (Figure 4e, h, i). Experimental results indicated the suppression of macrophage inflammatory responses by DADS-nFeS treatment.

DADS-nFeS treatment alleviated the levels of oxidative stress and decreased the contents of 4-HNE, MDA, and SOD at 72 h after ICH.

In addition to the neuroinflammatory process, oxidative stress can results in serious SBI. To investigate whether DADS-nFeS could attenuate oxidative stress, we analysed the levels of 4-HNE. As a result, the immunostaining marker 4-HNE was found to be significantly increased in the ICH + vehicle group at 72 h after ICH compared with the sham group. The high levels of oxidative stress were suppressed in the two ICH + DADS-nFeS groups compared to the PBS administration group (Figure 5a). Additionally, 4-HNE was highly expressed in the ICH + vehicle group, as detected using western blot, while ICH + DADS-nFeS (post-treatment) showed better efficacy than ICH + DADS-nFeS (pre-treatment) in this experiment (Figure 5b, c). Previous studies demonstrated that the MDA content and SOD activity coordinated oxidative stress balance in the brain and were indicators of free radical damage[18, 19]. Therefore, to further verify the efficacy of DADS-nFeS on oxidative stress, we utilized MDA and SOD detection kits to measure the relative levels of MDA and SOD in the mouse brains. As shown in the results, the MDA content was evidently increased after ICH, but treatment with DADS-nFeS inhibited this trend (Figure 5d). In contrast, SOD activity was obviously improved in the ICH + DADS-nFeS group versus the ICH + vehicle group (Figure 5e). The above results indicated that DADS-nFeS could attenuate brain injury after ICH by restraining the levels of oxidative stress.

DADS-nFeS treatment suppressed neuronal cell apoptosis and improved the expression of Bcl-2 and Bax at 72 h after ICH.

In a previous experiment, we revealed that DADS-nFeS administration effectively alleviated F-JC-positive neurons in the perihaematomal area at 72 h after ICH (Figure 3c). For further evidence, TUNEL staining was carried out. The results indicated that TUNEL-positive cells were obviously increased in the ICH + vehicle group compared to the sham group at 72 h after ICH. However, DADS-nFeS treatment significantly

reduced the numbers of TUNEL-positive cells, and the two treatment groups showed no significant difference (Figure 5f, g). The expression of Bcl-2 and Bax was also measured at 72 h after ICH by western blots. The results demonstrated that the ratio of Bax/Bcl-2 was markedly decreased in the ipsilateral hemisphere in the DADS-nFeS group compared to the ICH + vehicle group (Figure 5h, i). Better efficacy was observed in the post-treatment group than in the pre-treatment group. These results suggested that neuroprotective and antiapoptotic effects could be mediated by DADS-nFeS.

DADS-nFeS treatment improved the short-term neurological deficits at 72 h after ICH.

In addition to the histopathological detection of mouse brains, behavioural indicators were also assessed to reveal functional motor recovery on Days 1 and 3 after ICH in mice. The corner turn test, forelimb placement test, and rotarod test were utilized in this experimental study. In the corner turn test, the right turns significantly increased in the ICH + vehicle group compared to the sham group, while DADS-nFeS treatment inhibited this trend on Day 1 and Day 3 (Figure 5j). ICH + DADS-nFeS (post-treatment) showed better efficacy on Day 3. Moreover, no significant difference was detected between the ICH + vehicle group and the two ICH + DADS-nFeS groups on Day 1 in the other two tests (Figure 5k, l). In the forelimb placement test, the mice notably placed the left paw on the countertop more times in the two ICH + DADS-nFeS groups than in the ICH + vehicle group on Day 3 (Figure 5k). Likewise, the mice treated with DADS-nFeS spent significantly more time on the rotarod than those in the ICH + vehicle group on Day 3 in the rotarod test (Figure 5l). As a result, motor disorder after ICH in mice could be improved by DADS-nFeS treatment, and DADS-nFeS (post-treatment) may attenuate the neurological deficits better than DADS-nFeS (pre-treatment).

DADS-nFeS treatment improved the long-term neurological deficits after ICH.

Relevant research demonstrates that stroke will result in various impairments in motor, sensory, learning, and memory domains in survivors[20, 21]. Hence, the Y maze test, rotarod test, and Morris water maze were performed to detect the long-term impairment of neurological function. In the Y maze test, the mice in the ICH + vehicle group spent more time remaining stationary than those in the sham group, while this trend was suppressed in the two ICH + DADS-nFeS groups (Figure 6a, b, c). In addition, the number of total arm entries and the percentage of spontaneous alternations were decreased in mice after ICH and increased by DADS-nFeS (Figure 6d, e). Of these, the DADS-nFeS preconditioning had no significant effect on the percentage of spontaneous alternation on Days 7 and 14 compared to that of the ICH + vehicle group. In the rotarod test, the time latency before falling on the rotarod was significantly shorter in the ICH + vehicle group than in the sham group in the first, second, and third weeks after ICH (Figure 6f). However, the falling latency was obviously increased with the administration of DADS-nFeS in the two treatment groups in the three stages. In the Morris water maze, the mice in the ICH + vehicle group spent less time in the target quadrant than those in the sham group on Day 25, while DADS-nFeS treatment improved the condition (Figure 6g, h). In addition, greater distances and more time were required to find the platform for the mice in the ICH + vehicle group on Days 21 to 25. However, a significant reduction occurred in escape latency and swim distance in the two DADS-nFeS treatment groups (Figure 6i, j). Thus, DADS-nFeS (post-treatment) but not DADS-nFeS (pre-treatment) had better efficacy over a long period of motor functional rehabilitation. These results suggest that DADS-nFeS may improve long-term poststroke cognitive performance.

Discussion

Haemorrhagic stroke is a severe disease with high mortality and poor outcomes for patients. Previous studies have illustrated that intracerebral haematoma, neuroinflammation, and oxidative stress are closely related to neurodegeneration and neurological dysfunction[22, 23]. Consequently, decreasing the haematoma volume

and inhibiting neuroinflammation and oxidative stress have been proven to effectively alleviate this condition.

This is the first study to detect the therapeutic potential of DADS-nFeS against intracerebral haemorrhage in mice. In the current study, we first investigated the drug toxicity of three different dosages of DADS-nFeS in mice after ICH and then ascertained the comparatively better dosage of DADS-nFeS. Second, we explored the neuroprotective effects of gavage administration of DADS-nFeS on space-occupying haematoma lesions, neuroinflammation, oxidative stress, neuronal apoptosis, and neurobehavioural parameters in mice with collagenase-induced intracerebral haemorrhage. We demonstrated that oral DADS-nFeS evidently decreased the haematoma volume, suppressed the activation of microglia and astrocytes, reduced lipid peroxidation products, enhanced SOD activity, and inhibited neuronal apoptosis in the perihaematomal area. Correspondingly, our results also showed that the expression of Iba-1, GFAP, TNF-α, IL-1β, 4-HNE, and Bax was downregulated by the application of DADS-nFeS. In addition, we further performed short- and long-term neurobehavioural and neurocognitive tests, and obvious improvement was observed in multiple phases. Finally, this study suggested that the gavage administration of DADS-nFeS may alleviate the PBI and SBI, which in turn protect neurons from apoptosis and improve neurological functions.

Neuroinflammation plays an important role in SBI. Of these, astrocytes and microglia, as immune cells in the brain, are important mediators that modulate neuroinflammation. Previous studies indicated that microglia can be activated and accumulate at the perihaematomal area in a short time after ICH[24, 25]. Moreover, microglia have two types that can release various inflammation-related cytokines. Of these, M1 microglia can release TNF-α, IL-1β, and iNOS, while M2 microglia can release brain-derived neurotrophic factor (BDNF) and anti-inflammatory cytokines[26]. Therefore, proinflammatory cytokines constantly exacerbate neuroinflammation and become classic inflammatory markers. Astrocytes used to be viewed as an integral component of the blood brain barrier (BBB). Numerous studies

have examined its functions in the BBB, while few studies have focused on its neuroinflammatory abilities. Some studies found that excessive activation of astrocytes can stimulate proinflammatory cytokine release, activate the proinflammatory pathways of glial cells (microglia, oligodendrocytes), and contribute to neuronal excitotoxicity[27, 28]. Consequently, inhibiting the excessive activation of astrocytes can significantly attenuate inflammatory processes. Our results indicated that the activation of microglia and astrocytes was obviously suppressed by DADS-nFeS treatment. Moreover, the content of inflammatory cytokines decreased in the perihaematomal area. Our results confirmed that DADS-nFeS alleviated neuroinflammation and decreased neuronal apoptosis by decreasing glial cell activity and the expression of inflammatory cytokines.

One of the main mechanisms of brain injury following haemorrhagic apoplexy is oxidative stress mediated by ROS. Due to the space-occupying lesion of haematoma after ICH, the neurovascular structures experience heavy damage, and various cytotoxic molecules extravasate. Of these, haeme, as the major ingredient of haemoglobin, can release excessive ferrous iron and catalyse a mass of hydroxyl radicals[29–31], which is a dangerous type of ROS leading to severe lipid peroxidation and cell apoptosis. Moreover, as an unstable marker of oxidative stress, lipid peroxides often decompose to form MDA and 4-HNE[32]. SOD is closely related to oxygen radical detoxification. Numerous studies have indicated that some neuroprotective drugs can increase the activity of SOD and decrease the accumulation of ROS in the lesion area[33–35]. In contrast, the lack of SOD activation will lead to a high level of ROS and cause serious neuronal injury[36–38]. In addition, our previous studies have suggested that DADS-nFeS is fairly stable and displays high peroxidase-like activity[11]. In our results, with the administration of DADS-nFeS, the MDA content and the expression of 4-HNE were obviously decreased, and local SOD activation was significantly increased. Therefore, it seemed that DADS-nFeS can synergistically decrease the accumulation of ROS and inhibit lipid peroxidation by activating its peroxidase-like activity and improving local SOD activation, which

eventually suppresses oxidative stress.

DADS-nFeS is a novel nano-iron sulphide converted from natural organosulfur compounds fabricated by Xu et al. This conversion endows iron-based nanoparticles with various functions and higher peroxidase-like activity. We found that these nanoiron sulphides have the potential to become an alternative for treating ICH and display the following characteristics: (1) DADS-nFeS is a nanoparticle with high stability and dispersibility in the solvent, which makes it suited for in vivo treatment and long-term use. (2) DADS-nFeS attenuates neuroinflammation and oxidative stress partly by constantly releasing hydrogen polysulphanes. These hydrogen polysulfanes can easily penetrate the biofilm matrix, benefiting from good diffusibility[39]. (3) The peroxidase-like activity of nanoiron sulphides can accelerate the release of polysulfanes and result in a synergistic effect, which in turn enhances the efficacy[11]. In addition, a small number of studies have begun to investigate the role of hydrogen sulphide in cerebral haemorrhage and verified that it has a certain neuroprotective effect, but the mechanism is still unclear[40–42]. In this study, we found that DADS-nFeS obviously alleviated cell apoptosis and improved neurological deficits in mice after ICH. As a notable feature of ICH, neuronal apoptosis is regulated by the expression of Bcl-2 and Bax levels and strongly associated with unfavourable outcomes of patients after ICH[43, 44]. Western blot analysis demonstrated that the ratio of Bax/Bcl-2 resulting from haematoma was reduced by DADS-nFeS, which was in line with the TUNEL staining results. Correspondingly, DADS-nFeS treatment also had a positive effect on motor, spatial learning, and memory functions in mice on Days 3, 7, 14, and 21 after ICH.

Taken together, the present study preliminarily revealed some potential mechanisms of the anti-inflammatory, antioxidative stress, and antiapoptotic effects of DADS-nFeS after ICH. The in-depth mechanisms merit further explorations. Some studies have shown that hydrogen sulphides may be strongly connected with PI3K/Akt and promote the nuclear translocation of NF-κB[45, 46]. Other studies demonstrated that as a downstream effector of PTEN, the PI3K/Akt signalling

pathway participates in macrophage polarization and that TLR4/NF-κB pathway-related proteins mediate microglial polarization from M1 to M2[47–49]. Hence, it is worth further investigating the specific mechanism by which DADS-nFeS regulates microglial polarization, with hydrogen sulphides as a positive control, which is ongoing in another study from our group.

There are several limitations in our study. First, the collagenase-induced ICH model and the autologous blood-induced ICH model are the most often used ICH models. Both models have their own advantages. We chose the former due to the better disease process. However, the latter can better mimic the effects of the haematoma mass, which should not be ignored[40]. Thus, the efficacy of DADS-nFeS should be verified in different models in future studies. Second, our immunofluorescence staining and western blot results showed that DADS-nFeS can affect the activation of microglia and astrocytes. Of these, astrocytes, as primary cells, can produce hydrogen sulphides, which in turn regulate other glial cells[40]. The interactions between exogenous hydrogen polysulphanes released from DADS-nFeS and endogenous hydrogen sulphides from astrocytes have not yet been clarified. Therefore, further studies are required to explore the neuroprotective effects of DADS-nFeS on other CNS cells against SBI after ICH. Third, in the current study, we confirmed that DADS-nFeS and its product can synergistically suppress inflammation, oxidative stress, and apoptosis. However, we did not compare the efficacy between DADS-nFeS and hydrogen sulphides. In summary, it is valuable and necessary to use hydrogen sulphides as a positive control in further studies. Finally, recent studies indicated that prognosis after ICH was determined by two major risk factors, sex and age[50]. Our present study utilized only male C57BL/6 mice aged 8 to 12 weeks. Female sex and age groups were not evaluated in this experiment. Hence, further studies should include females and age groups to confirm the curative efficacy of DADS-nFeS in mice after ICH.

Conclusion

In conclusion, we preliminarily demonstrated that gavage administration of DADS-nFeS decreased haematoma volume and alleviated neuroinflammation, oxidative stress, and neuronal apoptosis, at least in part by repressing the activation of microglia and astrocytes and enhancing local SOD activity. Moreover, post-treatment had a better efficacy than pre-treatment. Therefore, based on the above advantages and large-scale preparation at low cost, DADS-nFeS may serve as a potential therapeutic strategy used as a dietary regimen against central nervous system diseases.

Abbreviations

ICH: Intracerebral haemorrhage; DADS-nFeS: Diallyl disulfide nFeS; F-JC : Fluoro-Jade C; TUNEL: Terminal deoxynucleotidyl transferase dUTP nick end labelling; MDA: Malondialdehyde; SOD: Superoxide dismutase; Iba-1: Ionized calcium binding adapter molecule 1; GFAP: Glial fibrillary acidic protein; TNF-α: Tumor necrosis factor-α; IL-1β: Interleukin-1β; 4-HNE: 4-hydroxynonenal; Bcl-2: B-cell lymphoma-2; Bax: Bcl-2-associated X; PBI: Primary brain injury; SBI: Secondary brain injury; ROS: Reactive oxygen species; H&E: Hematoxylin-eosin; PBS: Phosphate-buffered saline; PFA: Paraformaldehyde; OCT: Optimal cutting temperature; BSA: Bovine serum albumin; DAPI: 4',6-diamidino-2-phenylindole; PVDF: Polyvinylidene fluoride; GAPDH: Glyceraldehyde phosphate dehydrogenase; ANOVA: Analysis of variance; BDNF: Brain-derived neurotrophic factor; BBB: Blood brain barrier; PI3K: Phosphatidylinositol 3-kinase; Akt: Protein kinase B; NF-κB: Nuclear factor kappa-B; PTEN: Gene of phosphate and tension homology deleted on chromsome ten.

Declarations

Ethics approval and consent to participate

All experimental procedures were in accordance with the National Institutes of Health Guidelines for the Care and Use of Laboratory Animals and approved by the

Yangzhou University Institutional Animal Care and Use Committee.

Consent for publication

Not applicable.

Availability of data and materials

The datasets used and/or analysed during the current study are available from the corresponding author on reasonable request.

Competing interests

The authors declare that they have no competing interests.

Funding

This study was supported by the National Key Research Program of China (2016YFE0126000) and projects supported by the "Six Talent Peaks" in Jiangsu Province (WSN-082).

Authors' contributions

SZ, TQX, and JYL designed the experiment and prepared the manuscript. ZBX provided materials. TQX, JYL and ZBX provided technical guidance. XTQ, YY, JYL, and ZBX worked on the manuscript revision. SZ, WWZ, YJX, JWZ and CHT participated in the experiment and data analysis. The authors read and approved the final manuscript.

Acknowledgements

Not applicable.

Author details

[1]School of Nursing, Yangzhou University, Yangzhou, 225001, China. [2]School of

Medicine, Yangzhou University, Yangzhou, 225001, China. [3]Institute of Translational Medicine, Medical College, Yangzhou University, Yangzhou, 225001, China. [4]Jiangsu Key Laboratory of Integrated Traditional Chinese and Western Medicine for Prevention and Treatment of Senile Diseases, Yangzhou University, Yangzhou, 225001, China.

References

1. Li Z, Li M, Shi SX, Yao N, Cheng X, Guo A, Zhu Z, Zhang X, Liu Q (2020) Brain transforms natural killer cells that exacerbate brain edema after intracerebral hemorrhage. J Exp Med. https://doi.org/10.1084/jem.20200213
2. Deng S, Sherchan P, Jin P, Huang L, Travis Z, Zhang JH, Gong Y, Tang J (2020) Recombinant CCL17 Enhances Hematoma Resolution and Activation of CCR4/ERK/Nrf2/CD163 Signaling Pathway After Intracerebral Hemorrhage in Mice. Neurotherapeutics 17:1940–1953
3. Zeng J, Chen Y, Ding R, Feng L, Fu Z, Yang S, Deng X, Xie Z, Zheng S (2017) Isoliquiritigenin alleviates early brain injury after experimental intracerebral hemorrhage via suppressing ROS- and/or NF-KB-mediated NLRP3 inflammasome activation by promoting Nrf2 antioxidant pathway. J Neuroinflammation 14:1–19
4. Budinich CS, Chen H, Lowe D, Rosenberger JG, Bernstock JD, McCabe JT (2012) Mouse brain PSA-NCAM levels are altered by graded-controlled cortical impact injury. Neural Plast. https://doi.org/10.1155/2012/378307
5. Yamada M, Hayashi H, Suzuki K, Sato S, Inoue D, Iwatani Y, Ohata M, Yuan B, Takagi N (2019) Furin-mediated cleavage of LRP1 and increase in ICD of LRP1 after cerebral ischemia and after exposure of cultured neurons to NMDA. Sci Rep 9:1–12
6. Mendelow AD, Gregson BA, Fernandes HM, Murray GD, Teasdale GM, Terence Hope D, Karimi A, Shaw MDM, Barer DH (2005) Early surgery versus initial conservative treatment in patients with spontaneous supratentorial intracerebral haematomas in the International Surgical Trial in Intracerebral Haemorrhage (STICH): A randomised trial. Lancet 365:387–397
7. Zhang Z, Cho S, Rehni AK, Quero HN, Dave KR, Zhao W (2020) Automated Assessment of Hematoma Volume of Rodents Subjected to Experimental Intracerebral Hemorrhagic Stroke by Bayes Segmentation Approach. Transl Stroke Res 11:789–798

8. Liu J, Guo X, Zhao Z, Li B, Qin J, Peng Z, He G, Brett DJL, Wang R, Lu X (2020) Fe3S4 nanoparticles for arterial inflammation therapy: Integration of magnetic hyperthermia and photothermal treatment. Appl Mater Today. https://doi.org/10.1016/j.apmt.2019.100457
9. Yuan Y, Wang L, Gao L (2020) Nano-Sized Iron Sulfide: Structure, Synthesis, Properties, and Biomedical Applications. Front Chem 8:1–16
10. Mracsko E, Veltkamp R (2014) Neuroinflammation after intracerebral hemorrhage. Front Cell Neurosci 8:1–13
11. Xu Z, Qiu Z, Liu Q, et al (2018) Converting organosulfur compounds to inorganic polysulfides against resistant bacterial infections. Nat Commun 9:1–13
12. Tang X, Yan K, Wang Y, Wang Y, Chen H, Xu J, Lu Y, Wang X, Liang J, Zhang X (2020) Activation of PPAR-β/δ Attenuates Brain Injury by Suppressing Inflammation and Apoptosis in a Collagenase-Induced Intracerebral Hemorrhage Mouse Model. Neurochem Res 45:837–850
13. Xiong TQ, Chen LM, Gui Y, Jiang T, Tan BH, Li SL, Li YC (2019) The effects of epothilone D on microtubule degradation and delayed neuronal death in the hippocampus following transient global ischemia. J Chem Neuroanat 98:17–26
14. Feng L, Dou C, Xia Y, et al (2021) Neutrophil-like Cell-Membrane-Coated Nanozyme Therapy for Ischemic Brain Damage and Long-Term Neurological Functional Recovery. ACS Nano 15:2263–2280
15. Chen S, Peng J, Sherchan P, et al (2020) TREM2 activation attenuates neuroinflammation and neuronal apoptosis via PI3K/Akt pathway after intracerebral hemorrhage in mice. J Neuroinflammation 17:1–16
16. Zheng L, Yu M, Lin R, Wang Y, Zhuo Z, Cheng N, Wang M, Tang Y, Wang L, Hou ST (2020) Rhythmic light flicker rescues hippocampal low gamma and protects ischemic neurons by enhancing presynaptic plasticity. Nat Commun. https://doi.org/10.1038/s41467-020-16826-0

17. Ohgomori T, Jinno S (2020) Modulation of neuropathology and cognitive deficits by lipopolysaccharide preconditioning in a mouse pilocarpine model of status epilepticus. Neuropharmacology 176:108227
18. Liu Y, Zhang L, Liang J (2015) Activation of the Nrf2 defense pathway contributes to neuroprotective effects of phloretin on oxidative stress injury after cerebral ischemia/reperfusion in rats. J Neurol Sci 351:88–92
19. Abd-Elsameea AA, Moustaf AA, Mohamed AM (2014) Modulation of the oxidative stress by metformin in the cerebrum of rats exposed to global cerebral ischemia and ischemia/reperfusion. Eur Rev Med Pharmacol Sci 18:2387–2392
20. Chow WZ, Ong LK, Kluge MG, Gyawali P, Walker FR, Nilsson M (2020) Similar cognitive deficits in mice and humans in the chronic phase post-stroke identified using the touchscreen-based paired-associate learning task. Sci Rep 10:1–8
21. Houlton J, Zhou LYY, Barwick D, Gowing EK, Clarkson AN (2019) Stroke induces a BDNF-dependent improvement in cognitive flexibility in aged mice. Neural Plast. https://doi.org/10.1155/2019/1460890
22. Zhu F, Zi L, Yang P, Wei Y, Zhong R, Wang Y, You C, Li Y, Tian M, Gu Z (2021) Efficient Iron and ROS Nanoscavengers for Brain Protection after Intracerebral Hemorrhage. ACS Appl Mater Interfaces 13:9729–9738
23. Fu X, Zeng H, Zhao J, et al (2021) Inhibition of Dectin-1 Ameliorates Neuroinflammation by Regulating Microglia/Macrophage Phenotype After Intracerebral Hemorrhage in Mice. Transl Stroke Res. https://doi.org/10.1007/s12975-021-00889-2
24. Lan X, Han X, Li Q, Yang QW, Wang J (2017) Modulators of microglial activation and polarization after intracerebral haemorrhage. Nat Rev Neurol 13:420–433
25. Deng S, Jin P, Sherchan P, Liu S, Cui Y, Huang L, Zhang JH, Gong Y, Tang J (2021) Recombinant CCL17-dependent CCR4 activation alleviates

neuroinflammation and neuronal apoptosis through the PI3K/AKT/Foxo1 signaling pathway after ICH in mice. J Neuroinflammation 18:1–14

26. Lan X, Han X, Li Q, Li Q, Gao Y, Cheng T, Wan J, Zhu W, Wang J (2017) Pinocembrin protects hemorrhagic brain primarily by inhibiting toll-like receptor 4 and reducing M1 phenotype microglia. Brain Behav Immun 61:326–339

27. Linnerbauer M, Wheeler MA, Quintana FJ (2020) Astrocyte Crosstalk in CNS Inflammation. Neuron 108:608–622

28. Sanmarco LM, Wheeler MA, Gutiérrez-Vázquez C, et al (2021) Gut-licensed IFNγ+ NK cells drive LAMP1+TRAIL+ anti-inflammatory astrocytes. Nature 590:473–479

29. Goldstein L, Teng ZP, Zeserson E, Patel M, Regan RF (2003) Hemin induces an iron-dependent, oxidative injury to human neuron-like cells. J Neurosci Res 73:113–121

30. Kress GJ, Dineley KE, Reynolds IJ (2002) The relationship between intracellular free iron and cell injury in cultured neurons, astrocytes, and oligodendrocytes. J Neurosci 22:5848–5855

31. Yang Y, Xi Z, Xue Y, Ren J, Sun Y, Wang B, Zhong Z, Yang G yuan, Sun Q, Bian L (2017) Hemoglobin pretreatment endows rat cortical astrocytes resistance to hemin-induced toxicity via Nrf2/HO-1 pathway. Exp Cell Res 361:217–224

32. Liao D, Lv C, Cao L, Yao D, Wu Y, Long M, Liu N, Jiang P (2020) Curcumin Attenuates Chronic Unpredictable Mild Stress-Induced Depressive-Like Behaviors via Restoring Changes in Oxidative Stress and the Activation of Nrf2 Signaling Pathway in Rats. Oxid Med Cell Longev. https://doi.org/10.1155/2020/9268083

33. Jia D, Han B, Yang S, Zhao J (2014) Anemonin alleviates nerve injury after cerebral ischemia and reperfusion (I/R) in rats by improving antioxidant activities and inhibiting apoptosis pathway. J Mol Neurosci 53:271–279

751 34. Cheng C, Tang RQ, Xiong L, Hector RE, Bai FW, Zhao XQ (2018)
752 Association of improved oxidative stress tolerance and alleviation of glucose
753 repression with superior xylose-utilization capability by a natural isolate of
754 Saccharomyces cerevisiae. Biotechnol Biofuels 11:1–19
755 35. Duong TTH, Chami B, McMahon AC, Fong GM, Dennis JM, Freedman SB,
756 Witting PK (2014) Pre-treatment with the synthetic antioxidant T-butyl
757 bisphenol protects cerebral tissues from experimental ischemia reperfusion
758 injury. J Neurochem 130:733–747
759 36. Yu M, Chen R, Jia Z, Chen J, Lou J, Tang S, Zhang X (2016) MWCNTs
760 Induce ROS Generation, ERK Phosphorylation, and SOD-2 Expression in
761 Human Mesothelial Cells. Int J Toxicol 35:17–26
762 37. Wanchao S, Chen M, Zhiguo S, Futang X, Mengmeng S (2018) Protective
763 effect and mechanism of lactobacillus on cerebral ischemia reperfusion injury
764 in rats. Brazilian J Med Biol Res 51:5275–5282
765 38. Dai Y, Zhang H, Zhang J, Yan M (2018) Isoquercetin attenuates oxidative
766 stress and neuronal apoptosis after ischemia/reperfusion injury via
767 Nrf2-mediated inhibition of the NOX4/ROS/NF-κB pathway. Chem Biol
768 Interact 284:32–40
769 39. Riahi S, Rowley CN (2014) Why can hydrogen sulfide permeate cell
770 membranes? J Am Chem Soc 136:15111–15113
771 40. Zhang J, Shan H, Tao L, Zhang M (2020) Biological Effects of Hydrogen
772 Sulfide and Its Protective Role in Intracerebral Hemorrhage. J Mol Neurosci
773 70:2020–2030
774 41. Zhao H, Pan P, Yang Y, et al (2017) Endogenous hydrogen sulphide attenuates
775 NLRP3 inflammasome-mediated neuroinflammation by suppressing the P2X7
776 receptor after intracerebral haemorrhage in rats. J Neuroinflammation 14:1–18
777 42. Shan H, Qiu J, Chang P, et al (2019) Exogenous Hydrogen Sulfide Offers
778 Neuroprotection on Intracerebral Hemorrhage Injury Through Modulating
779 Endogenous H2S Metabolism in Mice. Front Cell Neurosci 13:1–14

43. Kim JH, Meng HW, He MT, Choi JM, Lee D, Cho EJ (2020) Krill Oil Attenuates Cognitive Impairment by the Regulation of Oxidative Stress and Neuronal Apoptosis in an Amyloid β-Induced Alzheimer's Disease Mouse Model. Molecules 25:3942
44. Bobinger T, Burkardt P, B. Huttner H, Manaenko A (2018) Programmed Cell Death after Intracerebral Hemorrhage. Curr Neuropharmacol 16:1267–1281
45. Zhang J, Shi C, Wang H, Gao C, Chang P, Chen X, Shan H, Zhang M, Tao L (2019) Hydrogen sulfide protects against cell damage through modulation of PI3K/Akt/Nrf2 signaling. Int J Biochem Cell Biol 117:105636
46. Jia G, Yu S, Sun W, Yang J, Wang Y, Qi Y, Chen Y (2020) Hydrogen Sulfide Attenuates Particulate Matter-Induced Emphysema and Airway Inflammation Through Nrf2-Dependent Manner. Front Pharmacol 11:1–13
47. Zhao D, Qin XP, Chen SF, Liao XY, Cheng J, Liu R, Lei Y, Zhang ZF, Wan Q (2019) PTEN Inhibition Protects Against Experimental Intracerebral Hemorrhage-Induced Brain Injury Through PTEN/E2F1/β-Catenin Pathway. Front Mol Neurosci 12:1–13
48. Zhou K, Zhong Q, Wang YC, et al (2017) Regulatory T cells ameliorate intracerebral hemorrhage-induced inflammatory injury by modulating microglia/macrophage polarization through the IL-10/GSK3β/PTEN axis. J Cereb Blood Flow Metab 37:967–979
49. Sun Z, Wu K, Gu L, Huang L, Zhuge Q, Yang S, Wang Z (2020) IGF-1R stimulation alters microglial polarization via TLR4/NF-κB pathway after cerebral hemorrhage in mice. Brain Res Bull 164:221–234
50. Hurn PD (2014) 2014 Thomas Willis award lecture: Sex, stroke, and innovation. Stroke 45:3725–3729

Figure Legends

Figure 1 Experimental design and animal groupings.

ICH, intracerebral haemorrhage; WB, western blot; F-JC: Fluoro-Jade C; TUNEL: terminal deoxynucleotidyl transferase dUTP nick end labelling; IF: immunofluorescence; MDA: malondialdehyde; SOD: superoxide dismutase.

Figure 2 Representative H&E staining photomicrographs of the heart, liver, spleen, lung, and kidney treated with PBS, DADS-nFeS (pre-treatment), and DADS-nFeS (post-treatment). Scale bar: 50 μm.

Figure 3 The effects of DADS-nFeS on haematoma volumes and neuronal survival at 72 h after ICH.

a Representative schematic diagrams of brain sections. **b** Quantitative analyses of haematoma volume based on morphometric measurements (n = 6/group). **c** Representative images of F-JC staining in the perihaematomal area. Scale bar: 100 μm. **d** Quantitative analyses of F-JC-positive neurons in the perihaematomal area (n = 6/group). **e** Representative images of Nissl staining in the perihaematomal area. Scale bar: 500 μm. **f** Quantitative analyses of surviving neurons in the perihaematomal area (n = 6/group). Error bars are represented as the mean ± SD. *$p < 0.05$ vs. sham, $^{@}p < 0.05$ vs. ICH + vehicle, $^{\#}p < 0.05$ vs. ICH + DADS-nFeS (25 mg/kg).

Figure 4 The effects of DADS-nFeS on activated microglia, astrocytes, and inflammation-related factors at 72 h after ICH.

a, b, c, d Representative images of immunofluorescence staining of Iba-1 and GFAP and quantitative analyses of Iba-1- and GFAP-positive cells in the perihaematomal area (n = 6/group). Scale bar: 100 μm. **e** Representative western blot bands showing Iba-1, GFAP, TNF-α, and IL-1β protein levels in the perihaematomal area. **f, g, h, i** Quantitative analyses of Iba-1, GFAP, TNF-α, and IL-1β protein levels in the perihaematomal area (n = 6/group). Error bars are represented as the mean ± SD. *p <

838 0.05 vs. sham, $^{@}p < 0.05$ vs. ICH + vehicle, $^{\#}p < 0.05$ vs. ICH + DADS-nFeS
839 (pre-treatment).
840
841 **Figure 5 The effects of DADS-nFeS on oxidative stress, neuronal apoptosis, and**
842 **short-term neurological deficits after ICH.**
843 **a** Representative image of immunofluorescence staining of 4-HNE at 72 h after ICH.
844 Scale bar: 100 μm. **b, c** Representative western blot bands and quantitative analyses
845 of 4-HNE at 72 h after ICH (n = 6/group). **d, e** Measurement of MDA content and
846 SOD activity in the perihaematomal area at 72 h after ICH (n = 6/group). **f, g**
847 Representative images of TUNEL staining and quantitative analyses of
848 TUNEL-positive cells in the perihaematomal area at 72 h after ICH (n = 6/group).
849 Scale bar: 100 μm. **h, i** Representative western blot bands and quantitative analyses of
850 Bcl-2 and Bax protein levels in the perihaematomal area at 72 h after ICH (n =
851 6/group). **j, k, l** Analyses of the corner turn test, forelimb placement test, and rotarod
852 test at 24 h and 72 h after ICH (n = 6/group). Error bars are represented as the mean ±
853 SD. $^{*}p < 0.05$ vs. sham, $^{@}p < 0.05$ vs. ICH + vehicle, $^{\#}p < 0.05$ vs. ICH +
854 DADS-nFeS (pre-treatment).
855
856 **Figure 6 The effects of DADS-nFeS on long-term neurological deficits after ICH.**
857 **a** Representative 8 min heat maps reflecting the average time cost in different parts of
858 the Y maze by each group. **b, c, d, e** Analyses of the quiescent time ratio, total
859 distance travelled, spontaneous alternation, and total arm entry on Days 7, 14, and 21
860 (n = 8/group). **f** Analyses of rotarod tests on Days 7, 14, and 21 (n = 8/group). **g**
861 Representative traces of the Morris water maze on Day 25 after ICH. **h** Analyses of
862 probe quadrant duration in the Morris water maze on Day 25 after ICH. **i, j** Analyses
863 of escape latency and swim distance of the Morris water maze on Days 21 to 25 after
864 ICH. Error bars are represented as the mean ± SD. $^{*}p < 0.05$ vs. sham, $^{@}p < 0.05$ vs.
865 ICH + vehicle, $^{\#}p < 0.05$ vs. ICH + DADS-nFeS (pre-treatment).

Figures

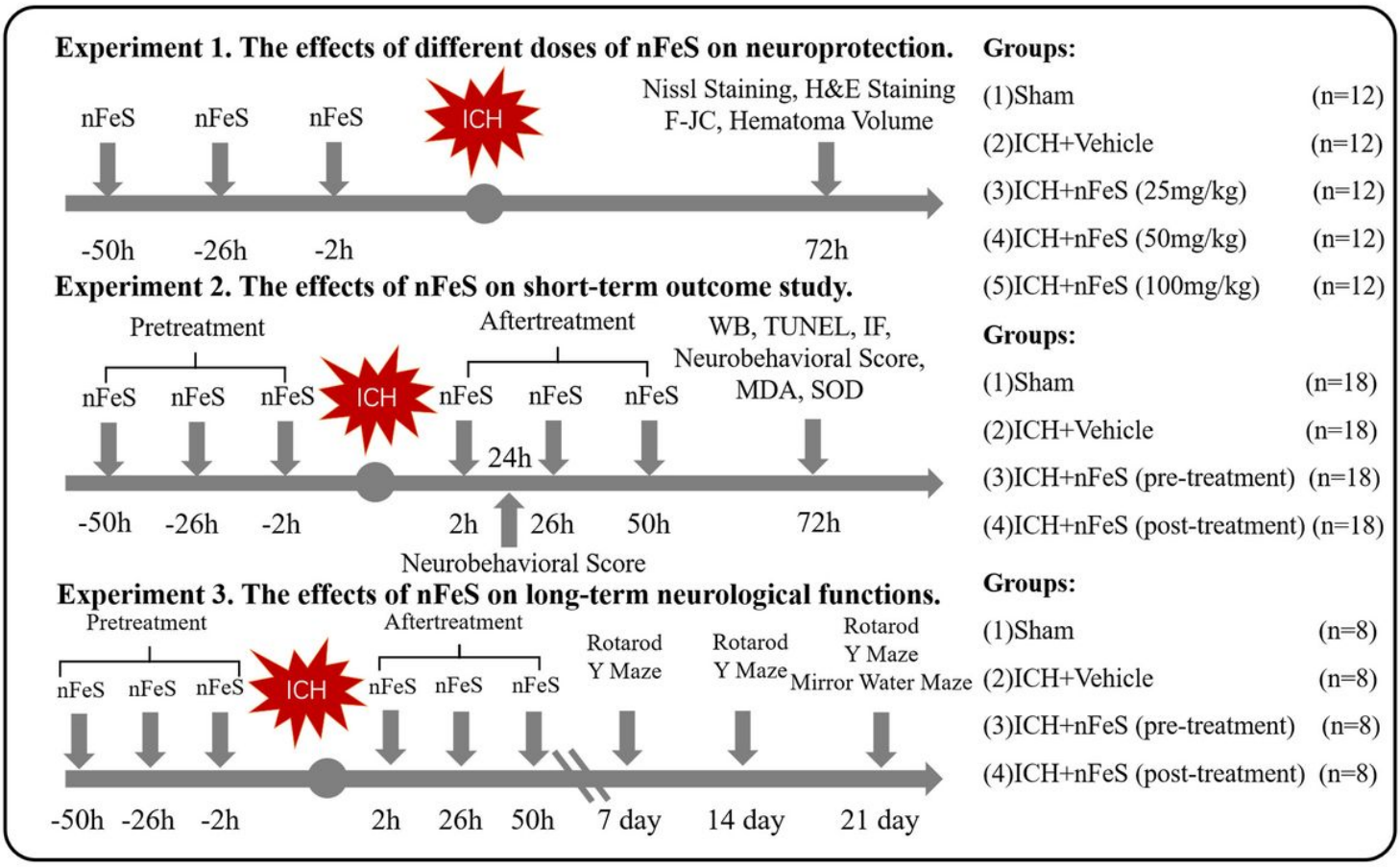

Figure 1

E x per imental design and animal groupings. ICH, intracerebral haemorrhage; WB, western blot; F JC : Fluoro Jade C ; TUNEL: terminal deo xynucleotidyl transferase dUTP nick end labelling; IF: immunofluorescence; MDA: malondialdehyde; SOD: superoxide di smut ase.

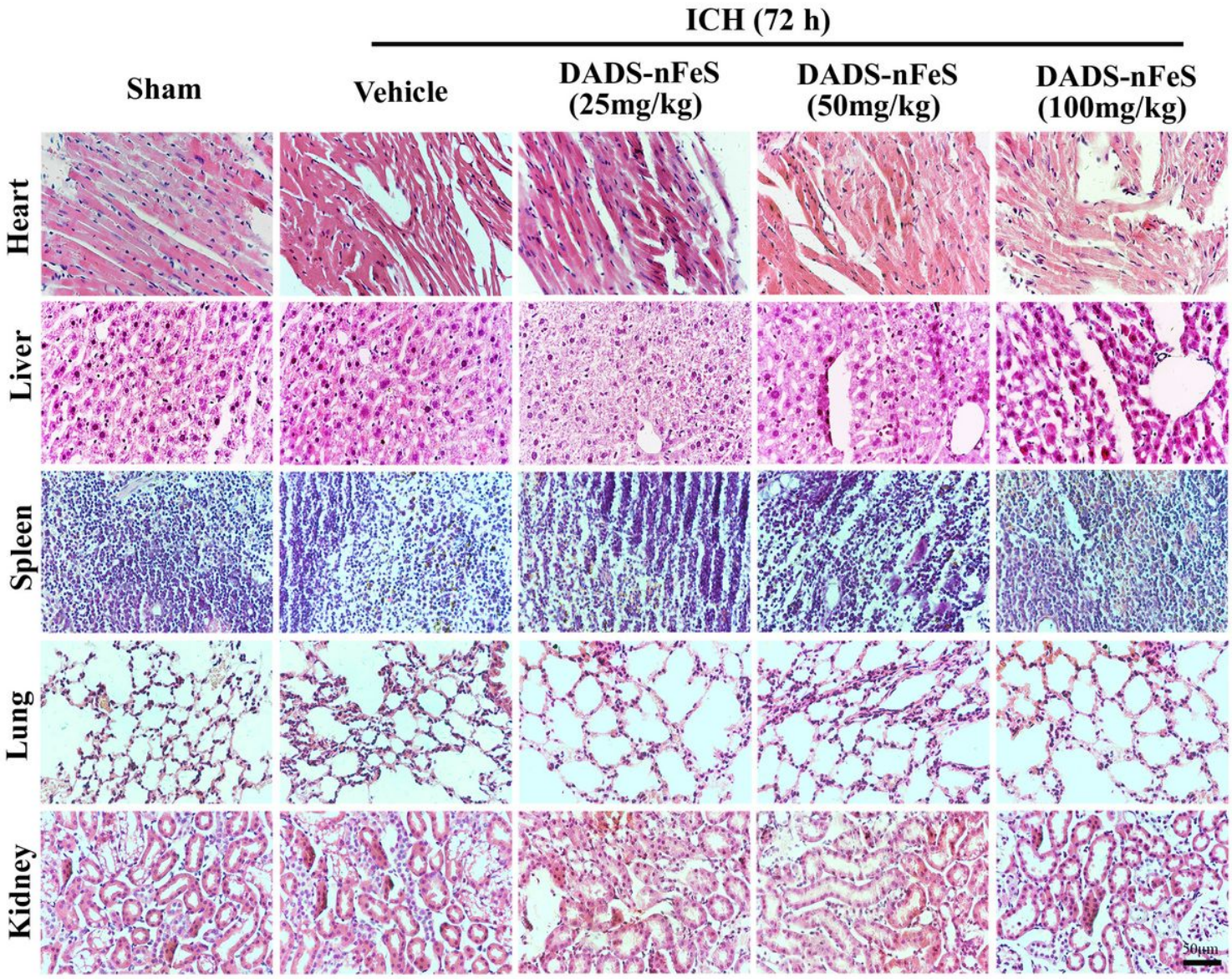

Figure 2

Representative H&E staining photomicrographs of the heart, liver, spleen, lung, and kidney treated with PBS, DADS nFeS (pr e treatment), and DADS nFeS post treatm ent). Scale bar: 50 μm.

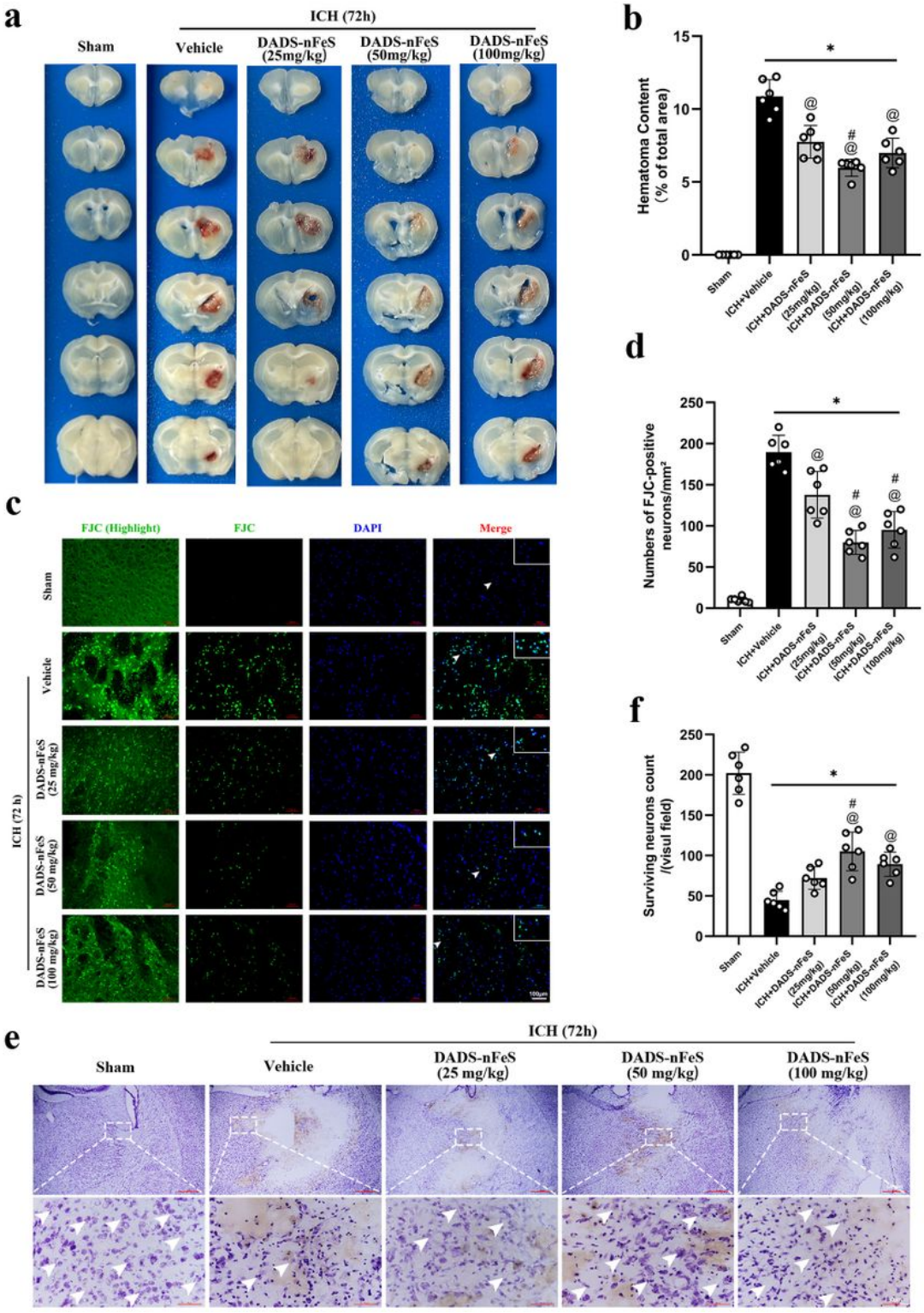

Figure 3

The effects of DADS nFeS on haematoma volumes and neuronal survival at 72 h after ICH. a Representative s chematic diagrams of brain sections. b Quantitative analyses of haematoma vo lume based on morphometric measurements (n = 6/group). c Rep resentative images of F JC staining in the perihaematomal area. Scale bar: 100 μm. d Quantitative analyses of F JC positive neurons in the perihaematomal area (n = 6/group). e Representative image s of Nissl staining in the perihaematoma l

area. Scale bar: 5 00 μm. f Quantitative analyses of surviving neurons in the perihaematomal area (n = 6/group). Error bars are represented as the mean ± SD. *p < 0.05 vs. s ham, p < 0.05 vs. ICH + v ehicle, p < 0.0 5 vs. ICH + DADS nFeS 25 mg/kg).

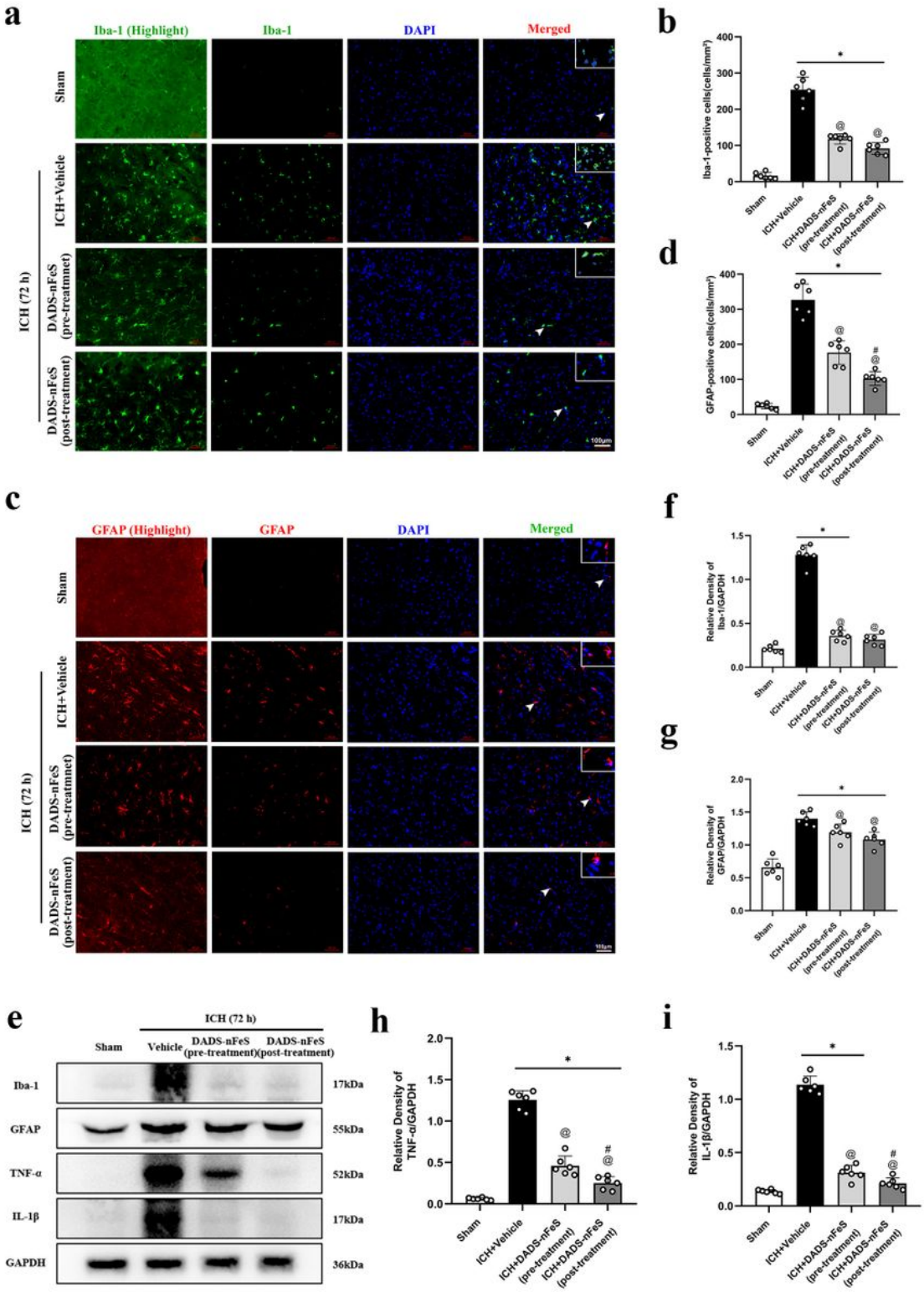

Figure 4

The effects of D ADS nFeS on a ctivated microglia, astrocytes, and inflammation related factors at 72 h after ICH. a, b, c, d Representative images of immunofluorescence staining of Iba 1 and GFAP and

quantitative analyses of Iba 1 and GFAP positive ce lls in the perihaema tomal area (n = 6/group). Scale bar: 100 μm. e Representative western blot bands showing Iba 1, GFAP, TNF α, and IL 1β protein levels in the perihaematomal area. f, g, h, i Quantitative analyses of Iba 1, GFAP, TNF α, and IL 1β protein levels in the perihaematomal area (n = 6/group). Error bars are represented as the mean ± SD. *p < 0.05 vs. s ham, p < 0.05 vs. ICH + v ehicle, p < 0.05 vs. ICH + DADS nFeS (pre treatment).

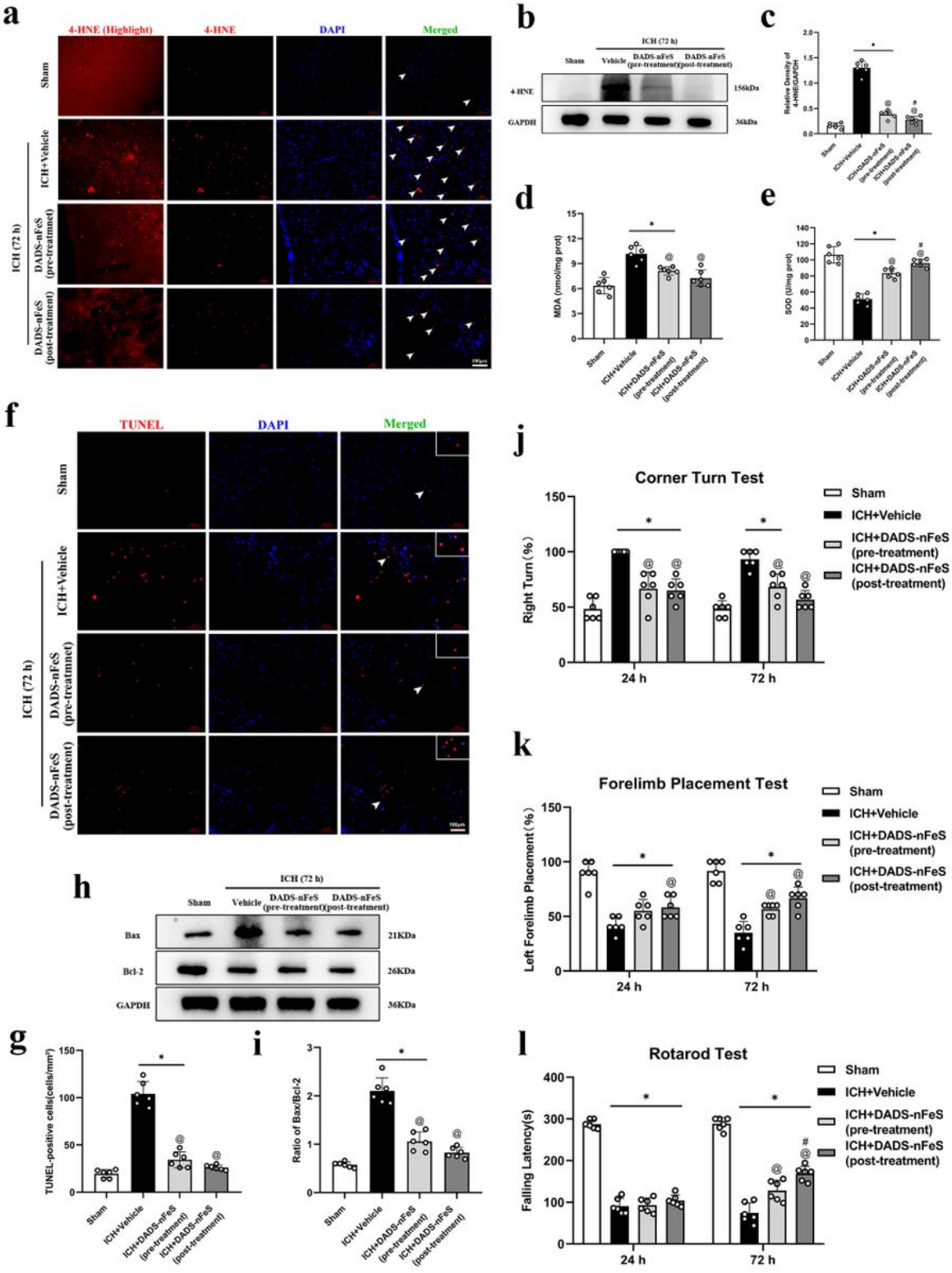

Figure 5

The effects of DADS nFeS on oxidative stress, neuronal a poptosis, and short term neurological deficits after ICH. a Representative image of immunofluorescence staining of 4 HNE at 72 h after ICH. Scale bar: 100 μm. b, c Representative western blot bands and quantitative analyses of 4 HNE at 72 h after ICH (n = 6/group). d, e Measureme nt of MDA content and SOD activity i n the perihaematomal area at 72 h after ICH (n = 6/group). f, g Representative images of TUNEL staining and quantitative analyses of TUNEL positive cells in the perihaematomal area at 72 h after ICH (n = 6/group). Scale bar: 100 μm. h, i Representative wes tern blot bands and quantitative analyses of Bcl 2 and Bax protein levels in the perihaematomal area at 72 h after ICH (n = 6/group) group). j, k, l Analyses of the corner turn test, forelimb placement test, and rotarod test at 24 h and 72 h after ICH (n = 6/grou p)p). Error bars are represented as the mean ± SD. *p < 0.05 vs. s ham, p < 0.05 vs. ICH + v ehicle, p < 0.05 vs. ICH + DADS nFeS pre treatment

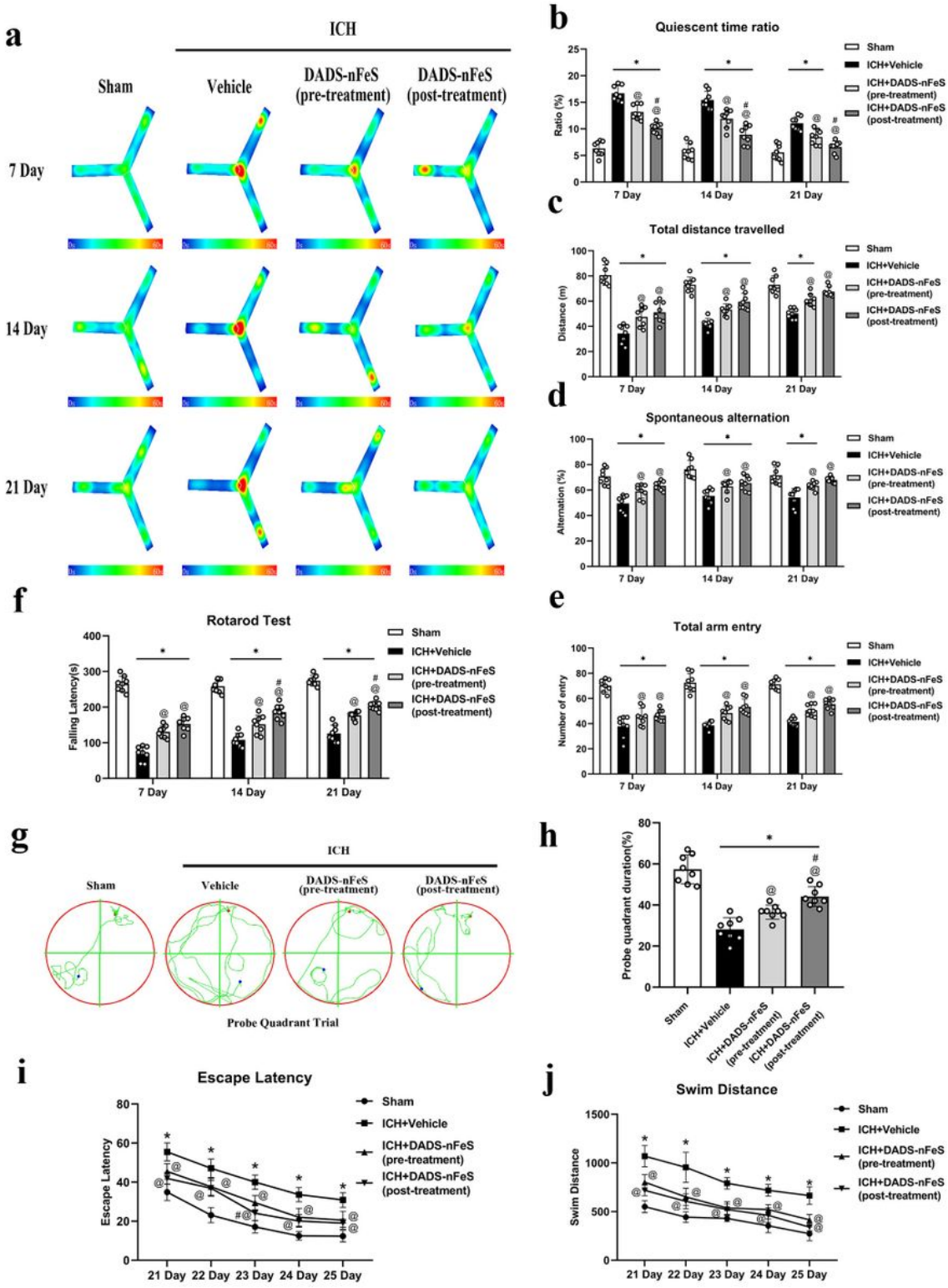

Figure 6

The effects of DADS nFeS on long term ne urological deficits after ICH. a Representative 8 min heat m aps reflecting the average time cost in different parts of the Y maze by each group. b, c, d, e Analyses of the quiescent time ratio, total distance travelled, spontaneous alternation, and total arm entry on Days 7, 14, and 21 (n = 8/ group). f Analyses of rotarod tests on Days 7, 14, and 21 (n = 8/group). g Representative traces of the Morris water maze on Day 25 after ICH. h Analyses of probe quadrant

duration in the Morris water maze on Day 25 after ICH. i, j Analyses of escape latency and swim distance of the Morris water maze on Days 21 to 25 after ICH. Error bars are represented as the mean ± SD. *p < 0.05 vs. s ham, p < 0.05 vs. ICH + v ehicle, p < 0.05 vs. ICH + DADS nFeS pre treatment

Supplementary Files

This is a list of supplementary files associated with this preprint. Click to download.

- Abbreviations.pdf
- EditingCertificate.pdf
- Westernblotsrawimagefiles.rar